Crystal-plasticity finite-element simulations of two-step loading of a ferrite-martensite dual phase steel sheet

Takayuki HAMA[1,a *], Yuto NAKATA[1,b], Naoki MIYAZAWA[1,c], Takashi MATSUNO[2,d], and Yoshitaka OKITSU[3,e]

[1]Graduate School of Energy Science, Kyoto University, Yoshida-Honmachi, Sakyo-ku, Kyoto, 606-8501, Japan

[2]Faculty of Engineering, Tottori University, 4-101 Koyama-cho-minami, Tottori, Tottori 680-8552, Japan

[3]Material Research Center, Honda R&D Co., Ltd., 4630 Shimotakanezawa, Haga-machi, Haga-gun, Tochigi, 321-3393, Japan

[a]hama@energy.kyoto-u.ac.jp, [b]nakata.yuto.64r@st.kyoto-u.ac.jp, [c]miyazawa.naoki.3n@kyoto-u.ac.jp, [d]matsu@tottori-u.ac.jp, [e]yoshitaka_okitsu@jp.honda

Keywords: Dual-Phase Steel, Two-Step Loading, Internal Stress

Abstract. Ferrite-martensite dual-phase (DP) steel sheets are widely used for structural components of automobiles. The macroscopic mechanical properties, including the yield stress and work hardening, of DP steel sheets are strongly affected by the microstructural properties, including the mechanical properties, volume fraction, and grain geometries of each phase. When DP steel sheets are subjected to tension in the rolling direction followed by tension in the transverse direction, the stress level after the strain-path change becomes smaller than that under monotonic tension in the transverse direction. However, the deformation mechanism of this behavior is not understood and open to discussion. In this study, experiments and crystal plasticity finite-element simulations of the two-step loading of a DP980 steel sheet are conducted, and the mechanisms that induce the stress decrease after the strain-path change are discussed. The results of crystal plasticity finite-element simulations well reproduced the experimental results of the stress-strain curves and the stress decrease after the strain-path change. The simulation results showed that the stress decrease occurred because of the following mechanisms. The tensile stresses during the first loading in the rolling direction were much smaller in the ferrite phase than in the martensite phase, which yielded compressive deviatoric stresses in the ferrite phase after unloading. This stress reversal in the ferrite phase upon unloading assisted macroscopic yielding after the strain-path change, decreasing the stress level.

Introduction

Ferrite-martensite dual-phase (DP) steel sheets are widely used for structural components of automobiles. The macroscopic mechanical properties, including the yield stress and work hardening, of DP steel sheets are strongly affected by the microstructural properties, including the mechanical properties, volume fraction, and grain geometries of each phase.

Previous studies reported that the stresses decrease when DP steel sheets are subjected to two-step loadings. Yu et al. [1] showed that, when DP steel sheets are subjected to tension in the rolling direction followed by tension in the transverse direction, the stress level after the strain-path change becomes smaller than that under monotonic tension in the transverse direction. Okitsu and Naito [2] reported similar results in different DP steel sheets. However, the deformation mechanisms of this behavior are not understood and open to discussion.

Crystal-plasticity models are powerful tools to investigate the effects of mesoscopic deformation on macroscopic deformation in crystalline materials; thus, they are extensively used also for DP steel sheets. Most of past studies [3,4] considered monotonic deformation, including tension and compression. There were also some studies for reverse loading processes [5,6]. However, the deformation behavior under two-step loadings has not been studied numerically.

In this study, experiments and crystal plasticity finite-element simulations of two-step loading of a DP steel sheet are conducted, and the mechanisms that induce the stress decrease after strain-path change are discussed.

Experimental Procedures

A 1.6-mm-thickness 980MPa-grade DP (DP980) steel sheet was used to conduct a two-step loading test. The volume fraction of the martensite phase was approximately 38.1%. The experimental procedures of a two-step loading test were according to a literature [7]. The large specimen shown in Fig. 1(a) was first stretched to a strain of 5% in the rolling direction (RD) and unloaded. Small specimens shown in Fig. 1(b) were then cut along the transverse direction (TD) from the gauge section of the prestrained large specimen. Subsequently, the small specimen was stretched. The stress-strain curve under the second-step loading was compared with the result of monotonic tension in the TD.

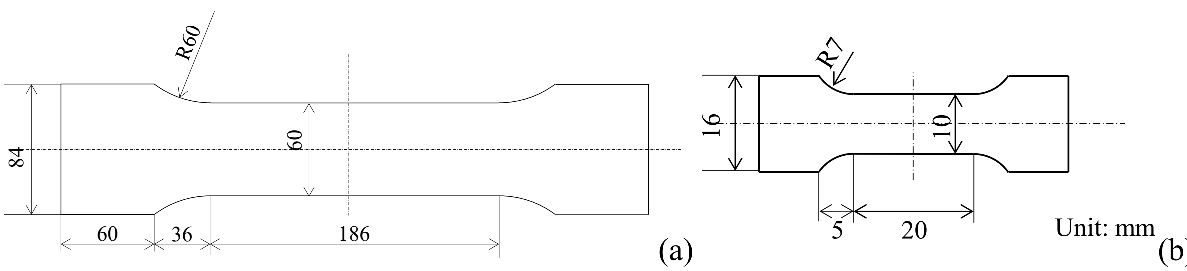

Figure 1 – Geometries of specimens for (a) first-step and (b) second-step loadings

Crystal-plasticity finite-element method

A crystal-plasticity finite-element method developed for metallic materials with a body-centered cubic (bcc) structure [8,9] was used to simulate the processes. Both ferrite and martensite phases were modeled to have the bcc structure. The {110} and {112} slip systems were considered. The slip rate of the αth slip system $\dot{\gamma}^{(\alpha)}$ is assumed to be related to the resolved shear stress $\tau^{(\alpha)}$ through the visco-plastic power law as follows.

$$\dot{\gamma}^{(\alpha)} = \dot{\gamma}_0 \left| \frac{\tau^{(\alpha)} - \tau_b^{(\alpha)}}{\tau_Y^{(\alpha)}} \right|^{\frac{1}{m}} \mathrm{sgn}\left(\tau^{(\alpha)} - \tau_b^{(\alpha)}\right), \qquad \tau^{(\alpha)} = \boldsymbol{s}^{(\alpha)} \cdot \sigma \cdot \boldsymbol{m}^{(\alpha)} \tag{1}$$

where $\dot{\gamma}_0$ is the reference strain rate, $\tau_\mathrm{Y}^{(\alpha)}$ is the slip resistance of the αth slip system with $\tau_Y^{(\alpha)} = \tau_0$ initially, and m is the strain rate sensitivity exponent. The evolution of slip resistance is given in the form:

$$\dot{\tau}_\mathrm{Y}^{(\alpha)} = \sum_\beta h(\bar{\gamma})\left|\dot{\gamma}^{(\beta)}\right| \tag{2}$$

where $h(\bar{\gamma})$ is the self-hardening rate given as a function of the accumulated slip $\bar{\gamma}$. The extended Voce hardening law is employed to represent the evolution of slip resistance as follows:

$$h(\bar{\gamma}) = \theta_1 + \left(\theta_0 - \theta_1 + \frac{\theta_0\theta_1}{\tau_1}\bar{\gamma}\right)\exp\left(-\frac{\theta_0\bar{\gamma}}{\tau_1}\right) \tag{3}$$

The accumulated slip is given in the time-integration form:

$$\bar{\gamma} = \sum_{\alpha} \int_0^t \left|\dot{\gamma}^{(\alpha)}\right| dt \tag{4}$$

$\tau_b^{(\alpha)}$ is the resolved back stress of the αth slip system and its evolution is given by:

$$\dot{\tau}_b^{(\alpha)} = c^{(\alpha)}\dot{\gamma}^{(\alpha)} - d^{(\alpha)}\tau_b^{(\alpha)}\left|\dot{\gamma}^{(\alpha)}\right| \tag{5}$$

where $c^{(\alpha)}$ and $d^{(\alpha)}$ are material parameters.

Fig. 2 shows the representative volume element (RVE) developed using the Dream.3D software [10]. The number of elements were 15x15x15=3375. The material parameters of Eq. (3) of the ferrite phase were determined to fit the hardening curve evaluated using the two-indenter method [11]. The back-stress parameters in Eq. (5) of the ferrite phase were determined according to the results of single-phase ferritic steel sheets. The parameters of the martensite phase were then identified to fit the stress-strain curve under reverse loading of the DP980 sheet in the RD using the ferrite parameters and RVE obtained earlier. The same parameters were assigned to the {110} and {112} slip systems. Fig. 3 shows the stress-strain curve of the DP980 steel sheet under reverse loading. The experiment of tension-compression reverse loading was conducted using comb-shaped dies [12, 13] to avoid buckling during compression. The simulation result well reproduced the experimental result.

Results and discussions

Fig. 4 shows the experimental and simulation results of the stress-strain curves upon the two-step loading. In the experimental results, the stress under monotonic tension is larger in the TD than in the RD, exhibiting anisotropic behavior. Comparing the results between TD monotonic tension and the second-step loading, the stress is smaller in the second-step loading than in monotonic loading, consistent with the literatures [1, 2]. The simulation results well reproduced the anisotropy between monotonic RD and TD tension and the stress decrease in the second-step loading.

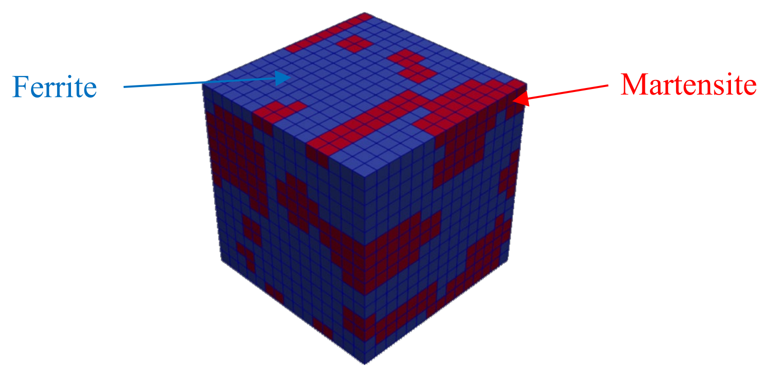

Figure 2 – RVE used in the simulations

To investigate the deformation mechanisms that yield the stress decrease in the second-step loading, the evolution of the deviatoric and hydrostatic stresses averaged over each phase during the first-step loading (tension in the RD) is shown in Fig. 5. The hydrostatic stresses are similar in the two phases and are negligible after unloading. By contrast, the absolute deviatoric stresses are apparently larger in the martensite phase than in the ferrite phase during loading.

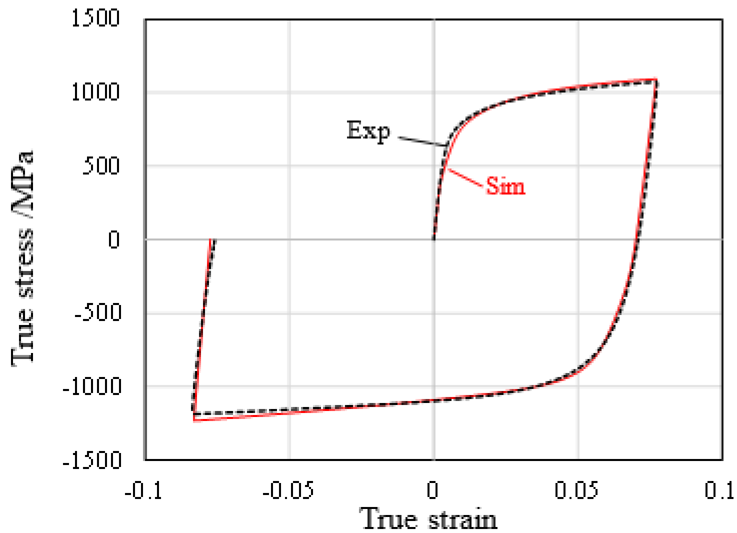

Figure 3 – Stress-strain curve of the DP980 sheet

Because the Young's modulus was assumed to be the same in the two phases, the absolute deviatoric stresses decreased along the same slope during unloading in both phases. Because of the large difference in the deviatoric-stress magnitude before unloading between the martensite and ferrite phases, the deviatoric stresses in the ferrite phase reached zero before the macroscopic unloading was completed. Moreover, the stresses kept on decreasing even after their signs were changed. By contrast, the large positive stresses remained in the martensite phase when the macroscopic unloading was completed. Consequently, when unloading was completed, the RD and TD components in the ferrite phase were positive and negative, respectively, whereas those in the martensite phase were still positive and negative, respectively.

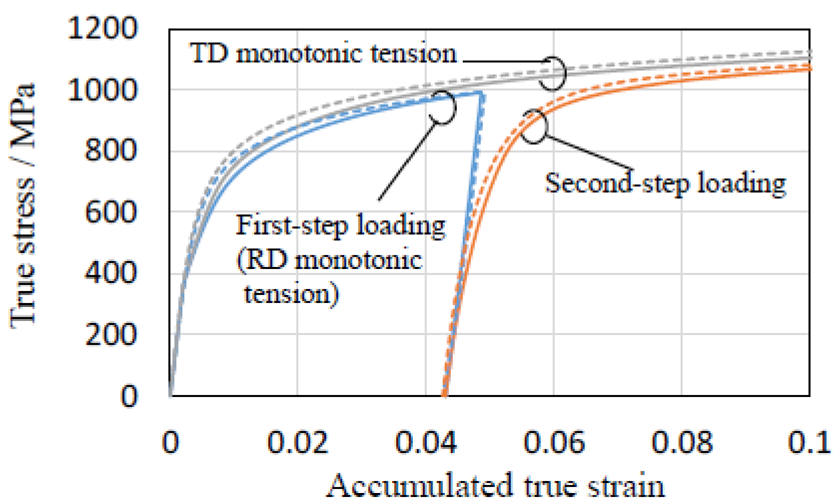

Figure 4 – Stress-strain curves under two-step loading. The solid and broken lines are the simulation and experimental results, respectively

These deviatoric stresses acted as the residual stresses at the beginning of second-step loading. When the sheet was stretched in the TD in the second-step loading, the large positive stresses of the TD component in the ferrite phase helped early macroscopic yielding because the plastic deformation at the early stage is primarily accommodated by the ferrite phase. Consequently, the stress level in the second-step loading became smaller than that of TD monotonic tension. These results suggest that the heterogeneous stress distributions that resulted from the large differences in the strength between the ferrite and martensite phases are a main factor that yield the stress decrease in the second-step loading.

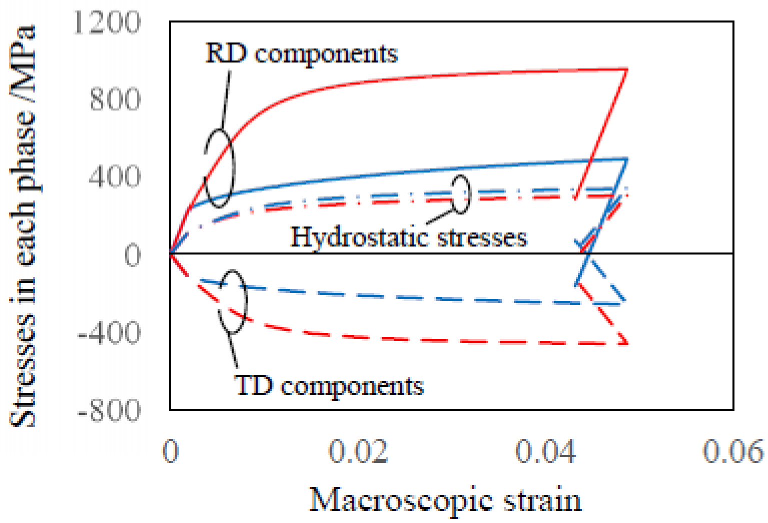

Figure 5 – Deviatoric and hydrostatic stress evolution during the first-step loading. The red and blue lines denote the results of martensite and ferrite phase, respectively

Conclusions

In this study, experiments and crystal plasticity finite-element simulations of two-step loading of a 980MPa-grade ferrite-martensite dual-phase steel sheet were conducted. In this test, the sheet was first stretched in the rolling direction, followed by tension in the transverse direction (TD). The mechanisms that yield stress decrease under second-step loading was studied. The results obtained in this study are as follows.

(1) Crystal-plasticity finite-element simulations well predicted the stress-strain curves obtained under two-step loading.

(2) Large differences in the stresses between the ferrite and martensite phases appeared in the first-step loading. These large differences resulted in positive residual stresses in the TD component in the ferrite phase after unloading. Consequently, the positive residual stresses in the ferrite phase helped macroscopic early yielding in the second-step loading, decreasing the macroscopic stress.

References

[1] H. Y. Yu, J. Y. Shen, Evolution of mechanical properties for a dual-phase steel subjected to different loading paths, Mater. Des., 63(2014), 412-418. http://dx.doi.org/10.1016/j.matdes.2014.06.003

[2] Y. Okitsu, T. Naito, Anisotropy in tensile properties of pre-strained various automotive sheet steels, Proc. 74th Japanese Joint Conf. Technol. Plasticity, Toyama, November, 2023, pp.7-8

[3] W. Liu, J. Lian, N. Aravas, S. Münstermann, A strategy for synthetic microstructure generation and crystal plasticity parameter calibration of fine-grain-structured dual-phase steel, Int. J. Plasticity, 126(2020), 102614. https://doi.org/10.1016/j.ijplas.2019.10.002

[4] T. Yalçinkaya, G. Ö. Güngör, S. O. Çakmak, C. Tekoğlu, A micromechanics based numerical investigation of dual phase steels, Proc. Struct. Integ., 21(2019), 61-72.

https://doi.org/10.1016/j.prostr.2019.12.087

[5] J. H. Kim, D. Kim, F. Barlat, M.-G. Lee, Crystal plasticity approach for predicting the Bauschinger effect in dual-phase steels, Mater. Sci. Eng. A, 539(2012), 259-270. https://doi.org/10.1016/j.msea.2012.01.092

[6] S. Daroju, T. Kuwabara, M. Knezevic, Experimental characterization and crystal plasticity modeling of dual-phase steels subjected to strain path reversals, Mech. Mater., 168(2022), 104293.

https://doi.org/10.1016/j.mechmat.2022.104293

[7] T. Hama, Y. Tanaka, M. Uratani, H. Takuda, Deformation behavior upon two-step loading in a magnesium alloy sheet, Int. J. Plasticity, 82(2016), 283-304. https://doi.org/10.1016/j.ijplas.2016.03.009

[8] T. Hama, H. Fujimoto, H. Takuda, Prediction of differential work-hardening behavior under biaxial tension of steel sheet using crystal plasticity models, Proc. Manuf., 15(2018), 1808-1815. https://doi.org/10.1016/j.promfg.2018.07.210

[9] T. Hama, M. Oka, T. Nishi, T. Matsuno, S. Hayashi, K. Takada, Y. Okitsu, Crystal plasticity finite-element simulation of non-uniform deformation behavior at grain level of ultralow carbon steel, ISIJ Int., 64(2024), 576-586. https://doi.org/10.2355/isijinternational.ISIJINT-2023-416

[10] M. A. Groeber, M. A. Jackson, DREAM.3D: a digital representation environment for the analysis of microstructure in 3D, Integr. Mater. Manuf. Innov. 3(2014), 5.

https://doi.org/10.1186/2193-9772-3-5

[11] N. Ogasawara, W. Makiguchi, M. Chiba, Plastic properties determination method using triangular pyramid indenters based on elastic solution and rigid/perfectly plastic solution, Trans. JSME A, 71(2005), 1406-1412. https://doi.org/10.1299/kikaia.71.1406

[12] T. Kuwabara, Advances in experiments on metal sheets and tubes in support of constitutive modeling and forming simulations, Int. J. Plast., 23 (2007) 385–419. https://doi.org/10.1016/j.ijplas.2006.06.003

[13] T. Hama, H. Nagao, A. Kobuki, H. Fujimoto, H. Takuda, Work-hardening and twinning behaviors in a commercially pure titanium sheet under various loading paths, Mater. Sci. Eng., A 620 (2015) 390–398. https://doi.org/10.1016/j. msea.2014.10.024